Choroidal and Retinal Changes After Systemic Adrenaline and Photodynamic Therapy in Non-Human Primates

Kai Xiong Cheong,[1] Veluchamy Amutha Barathi,[1–3] Kelvin Yi Chong Teo,[1] Usha Chakravarthy,[4] Sai Bo Bo Tun,[1] Joanna Marie Busoy,[1] Candice Ee Hua Ho,[1] Rupesh Agrawal,[1,2,5,6] Kanji Takahashi,[7] and Chui Ming Gemmy Cheung[1,2]

[1]Singapore Eye Research Institute, Singapore National Eye Centre, Singapore
[2]Ophthalmology & Visual Sciences Academic Clinical Program (Eye ACP), Duke-NUS Medical School, Singapore
[3]Department of Ophthalmology, Yong Loo Lin School of Medicine, National University of Singapore, Singapore
[4]School of Medicine, Dentistry and Biomedical Sciences, Queens University Belfast, Belfast, United Kingdom
[5]National Healthcare Group Eye Institute, Tan Tock Seng Hospital, Singapore, Singapore
[6]Moorfields Eye Hospital, NHS Foundation Trust, London, United Kingdom
[7]Department of Ophthalmology, Kansai Medical University, Hirakata, Osaka, Japan

Correspondence: Cheung Chui Ming Gemmy, Singapore Eye Research Institute, Singapore National Eye Centre, Singapore, 11 Third Hospital Avenue, 168751, Singapore; gemmy.cheung.c.m@snec.com.sg.

KXC and VAB contributed equally as joint first authors.

Received: July 24, 2020
Accepted: February 24, 2021
Published: March 17, 2021

Citation: Cheong KX, Barathi VA, Teo KYC, et al. Choroidal and retinal changes after systemic adrenaline and photodynamic therapy in non-human primates. *Invest Ophthalmol Vis Sci.* 2021;62(3):25. https://doi.org/10.1167/iovs.62.3.25

Purpose. To determine the tomographic, angiographic, and histologic changes in the choroid and retina of cynomolgus monkeys after systemic adrenaline and verteporfin photodynamic therapy (vPDT).

Methods. Six cynomolgus monkeys (12 eyes) were treated with vPDT only (n = 2), adrenaline only for eight weeks (n = 2), adrenaline for eight weeks with vPDT at week 4 (n = 4), and adrenaline for 12 weeks and vPDT at week 8 (n = 4). Spectral-domain optical coherence tomography, angiography, and autofluorescence were performed at baseline and every 14 days thereafter until 28 days after adrenaline therapy or vPDT. Choroid parameters included choroidal thickness (CT) changes and structural changes using semiautomated image binarization. Histology with light and electron microscopy was performed.

Results. Adrenaline resulted in subfoveal CT increase at week 4 compared with baseline (3.4%, $P = 0.010$), with further increase at week 8 (3.9%, $P = 0.007$). This correlated with choroidal luminal area increase (16.0% at week 8 compared with baseline, $P = 0.030$). Outer retinal changes included subretinal fluid, ellipsoid zone (EZ) disruption, photoreceptor elongation, and sub/intraretinal bright dots. Hypocyanescent spots surrounded by leakage was observed. Histology showed dilated choroidal vessels, intracytoplasmic vacuoles, and retinal pigment epithelium (RPE) enlarged basal infoldings. The vPDT decreased subfoveal CT at four weeks after vPDT (−7.5%, $P = 0.007$). This correlated with choroidal stromal area decrease (−18.0%, $P < 0.010$). Within the treatment spot, there was outer retinal atrophy, EZ disruption, irregular RPE thickening, intense hypoautofluorescence, hyperfluorescence, and hypocyanescence. On histology, there were outer retina, RPE, and choroid changes.

Conclusions. Adrenaline induces choroidal vessel dilation and CT increase. The vPDT decreases CT because of a reduction in choroidal stromal component.

Keywords: central serous chorioretinopathy, adrenaline, photodynamic therapy, retina, choroid

Central serous chorioretinopathy (CSCR) is a chorioretinal condition that is characterized by detachment of the neurosensory retina caused by leakage of fluid into the subretinal compartment through the retinal pigment epithelium (RPE).[1–4] CSCR is classically described to occur in young males with no underlying systemic conditions[5] and is often ascribed to several risk factors related to corticosteroid use,[6–7] high serum cortisol and catecholamine levels,[8] *Helicobacter pylori* infection,[9] genetic predisposition,[10] stress,[11] and type A personality.[12] Although the clinical characteristics of CSCR are well described, the pathophysiology is not as well understood.[1–3] Current evidence implicates a congested and hyperpermeable choroid that elevates tissue hydrostatic pressure beneath the RPE.[13,14] The barrier function of the RPE is thought to be overwhelmed under such circumstances, which in turn causes neurosensory detachments.[13,14]

Verteporfin (Visudyne; Novartis, Basel, Switzerland) photodynamic therapy (vPDT) is one of the treatment modalities for CSCR. Clinical studies have demonstrated accelerated resolution of subretinal fluid in response to vPDT.[15,16] As opposed to full-fluence vPDT, which was

Copyright 2021 The Authors

This work is licensed under a Creative Commons Attribution-NonCommercial-NoDerivatives 4.0 International License.

Downloaded from abstracts.iovs.org on 04/23/2024

Table 1. Study Schedule

Group	Number	Monkey(s)	Adrenaline	vPDT	Imaging Time Points
1	1	No. 6681	—	Baseline	Baseline After vPDT weeks 2 and 4
2	1	No. 6738	Day 1 to week 8	—	Baseline After administration of adrenaline weeks 2, 4, 6 and 8
3	2	No. 4824 No. 6756	Day 1 to week 8	Week 4	Baseline After administration of adrenaline weeks 2 and 4 After vPDT weeks 2 and 4
4	2	No. 6177 No. 6181	Day 1 to week 8	Week 8	Baseline After administration of adrenaline weeks 2, 4, 6 and 8 After vPDT weeks 2 and 4

initially advocated for treating choroidal neovascularization, half-fluence vPDT is believed to lead to less occlusive effect on the choriocapillaris.[17] However, the therapeutic mechanisms of vPDT in the context of CSCR are not well understood. Observations of reduced choroidal thickness (CT) on optical coherence tomography (OCT) and reduced hyperpermeability on indocyanine green angiography (ICGA) have led to suggestions that choroidal vasculature remodeling and choroidal congestion reduction are potential mechanisms.[18–20]

The lack of an animal model is one of the key challenges in achieving a better understanding of the pathophysiology of CSCR and the therapeutic mechanisms of vPDT. Previously, Yoshioka et al.[21–24] reported successful induction of fluorescein angiography (FA) leakage that is similar to that in CSCR after the intravenous (IV) administration of adrenaline in a non-human primate model. However, that study predated the development of OCT, and OCT was not performed. Therefore in this study we aim to elucidate the tomographic, angiographic, and histologic changes of the choroid and retina in cynomolgus monkeys after systemic adrenaline and vPDT. We specifically focused on spectral-domain OCT (SD-OCT) findings, which included microstructural changes within the outer retina and choroid. The current study incorporated evaluation of the choroidal structure represented by stromal or interstitial area of the choroid (SA), luminal or vascular area in the choroid (LA), and choroidal vascularity index (CVI) derived from the total choroidal area (TCA) and LA. This enabled us to further examine changes within the luminal versus stromal components of the choroid.

Methods

All procedures were carried out in the SingHealth Experimental Medicine Centre, which is licensed by the Agri-Food and Veterinary Authority of Singapore and is fully accredited by the Association for Assessment and Accreditation of Laboratory Animal Care International. The study adhered to the Association for Research in Vision and Ophthalmology Statement for the Use of Animals in Ophthalmic and Vision Research and the National Advisory Committee for Laboratory Animal Research guidelines in Singapore. Ethical approval was obtained from the SingHealth Institutional Animal Care and Use Committee (Approval Reference Number: 2018/SHS/1443).

Animals and Protocol

Six adult male cynomolgus macaque monkeys (*Macaca fascicularis*) of age three to six years and weight 3 to 7 kg were included into the study. All animals were given a comprehensive ocular examination, including that of the anterior segment and fundus, to exclude ocular disease.

The six animals representing 12 eyes were divided into four groups: group 1: vPDT (n = 2); group 2: systemic adrenaline for eight weeks (n = 2); group 3: systemic adrenaline for eight weeks and vPDT at week 4 (n = 4); and group 4: systemic adrenaline for 12 weeks and vPDT at week 8 (n = 4) (See Table 1).

General anesthesia was used during examination, imaging, and procedures, as described in previous studies.[21–24] This included intramuscular (IM) ketamine hydrochloride (20 mg/kg), IM acepromazine maleate (0.25 mg/kg), and IM atropine sulfate (0.125 mg/kg). The animals were euthanized at four weeks after the last procedure with IV phenobarbital (50 mg/kg) while under general anesthesia.

Systemic Adrenaline

In a previous experiment using systemic adrenaline, neurosensory detachment was noted on day 59.[21–24] Based on this, the duration of systemic adrenaline administration for groups 2, 3, and 4 were 60 days, 60 days, and 90 days, respectively. Adrenaline was administrated with the following protocol: day 1 to 7: IV 0.125 mg/kg; day 8 to 10: IV 0.125 mg/kg and IM 0.125 mg/kg, and Day 11 to end of follow-up: IV 0.375 mg/kg.

vPDT

The vPDT was performed at prespecified timepoints in groups 1, 3, and 4. Verteporfin (3 mg/m^2) was administrated intravenously to the animals through the saphenous vein. The settings were as follows: wavelength: 689 nm, light dosimetry: 300 mW/cm^2, fluence: 25 J/cm^2, treatment duration: 83 seconds. A 3000 µm spot was centered on the fovea.

Imaging

Imaging was performed at baseline and every 14 days thereafter until 28 days after adrenaline therapy or vPDT. See Table 1 for the protocol and imaging time points. At each imaging session, each animal underwent SD-OCT, FA, ICGA, and fundus autofluorescence (FAF).

SD-OCT was performed under standardized mesopic lighting conditions using Spectralis OCT (Heidelberg Engineering, Heidelberg, Germany). After adequate pupil dilation, a 25-line horizontal raster scan (20° × 20°, 6.0 mm × 6.0 mm) centered on the fovea was performed, with nine frames averaged in each OCT B-scan and enhanced-depth imaging mode enabled. SD-OCT images were obtained by

Investigative Ophthalmology & Visual Science

Downloaded from abstracts.iovs.org on 04/23/2024

trained optometrists, and acquisitions were repeated to obtain high-quality images. Images with a signal strength of six or less were excluded.

FA, ICGA, and FAF (excitation wavelength of 488 nm and a barrier filter at 500 nm) were performed with the Heidelberg Retina Angiograph 2 with confocal scanning laser ophthalmoscope (HRA+OCT Spectralis; Heidelberg Engineering). IV injections of 10% Sodium Fluorescein (0.1 ml/kg) and Indocyanine green (0.75 mg/kg) via the saphenous vein were performed. FA images were obtained every two to three seconds for the first 30 seconds, then at 45 seconds, and at one and five minutes. ICGA images were obtained every two to three seconds for the first 30 seconds, then at 45 seconds, and at one, five, 10, and 20 minutes.

Images were graded in duplicate by trained retinal specialists, who were masked to the treatment received by each animal. Where there were discrepancies, adjudication was overseen by a senior retinal specialist (CMGC).

Choroidal Thickness and Choroidal Vascularity Index

We measured CT and CVI[18,25–28] at three locations: subfoveal, superior to fovea, and inferior to fovea. The superior and inferior CT and CVI were measured at 10 OCT B-scans above and below the B-scan that corresponded to the fovea, respectively. The mean of the two extrafoveal locations of measurement was calculated. CT was measured using the caliper tool in the Heidelberg Explorer from the outer border of the RPE-basement membrane complex to the choroid-scleral interface.

To measure the CVI, image binarization was performed using public domain software ImageJ (version 1.53c; National Institutes of Health, Bethesda, MD, USA)[29,30] using the technique described by Agrawal et al.[25] and Nivison-Smith et al.[31] The polygon tool was used to select the TCA, which was added in the region of interest (ROI) manager. After the images were converted into eight bit, Niblack's auto local thresholding was applied that gave the mean pixel value with standard deviation for all the points. On the SD-OCT scans, the LA was highlighted by applying the color threshold. To determine the LA within the selected polygon, both the areas in ROI manager were selected and merged by the "AND" operation of ImageJ. The composite third area was added to the ROI manager. The first area represents the total of the choroid selected, and the third composite area is the LA. SA, which corresponds to the interstitial or stromal component of the choroid, was obtained by calculating the difference between TCA and LA. The CVI was calculated by dividing LA by TCA.

Histopathology and Immunohistochemistry

Enucleation was performed at five minutes postmortem, which was conducted at the end of the follow-up for all animals. Whole eyes were fixed in 10% neutral buffered formalin solution (Leica Surgipath; Leica Biosystems Richmond, Inc., Richmond, IL, USA) for 24 hours. The whole eye was then dissected to produce upper and lower halves of the posterior segment. The upper portion was dehydrated in increasing concentrations of ethanol, subjected to clearance in xylene, and embedded in paraffin (Leica-Surgipath; Leica Biosystems Richmond). Four-micron sections were cut with a rotary microtome (RM2255; Leica Biosystems Nussloch GmbH, Nussloch, Germany) and collected on POLYSINE microscope glass slides (Gerhard Menzel; Thermo Fisher Scientific, Waltham, MA, USA). The sections were dried in an oven at 37°C for at least 24 hours. To prepare the sections for histopathologic and immunohistochemical examination, the sections were heated on a 60°C heat plate, deparaffinized in xylene, and rehydrated in decreasing concentrations of ethanol. Hematoxylin and eosin staining was performed according to a standard procedure. A light microscope (Axioplan 2; Carl Zeiss Meditec GmbH, Oberkochen, Germany) was then used to examine the slides and capture the images.

In parallel, immunohistochemistry staining was performed using the BOND-III automated IHC Stainer with vascular endothelial growth factor primary antibody at 1:200 concentration (ab46154; Abcam, Cambridge, UK). For negative controls, the primary antibody was omitted. After washing the slides twice with 1× phosphate buffered saline solution (PBS) and once with 1× PBS containing 0.1% Tween for 10 minutes each, corresponding secondary antibodies (conjugated with Alexa 594; Molecular Probes, Eugene, OR, USA) were applied at a concentration of 1:1000 in 1× PBS and incubated for 90 minutes at room temperature. The slides were then washed twice with 1× PBS and once with 1× PBS containing 0.1% Tween for five minutes each. The slides were mounted with Prolong Diamond Antifade Reagent and DAPI (Invitrogen, Carlsbad, CA, USA) to visualize cell nuclei. A light microscope (Axioplan 2; Carl Zeiss Meditec GmbH) was used to examine the slides and images were captured. Experiments were repeated in duplicates for antibody staining.

Transmission Electron Microscopy

The lower portion of the posterior segments were fixed in a mixture of 2.5% Glutaraldehyde (EM Sciences, Pennsylvania, USA) and 2% Paraformaldehyde (PFA) (Sigma-Aldrich, Missouri, USA) in 1X PBS for two hours at 4°C and rinsed in 1X PBS thrice. Rinsed samples were post-fixed in 1% aqueous Osmium Tetroxide (OsO_4; EM Sciences, Pennsylvania, USA), dehydrated in increasing concentration of Ethanol, subjected to clearance in Acetone, and processed for Aradite resin infiltration and embedding. Semi-thin sections (0.5µm thick) were collected on POLYSINE™ microscope glass slides and stained in a solution of 0.5% Toluidine Blue O (Sigma-Aldrich, Missouri, USA) and 1% Sodium Borate (Sigma-Aldrich, Missouri, USA) dissolved in distilled water. The solution was filtered with hydrophobic membrane filter of a 25µm pore size prior to staining for light microscopy. Ultrathin sections (90nm thick) were contrast stained with Lead Citrate and examined under transmission electron microscopy (Tecnai Spirit G2 120kv; FEI Company, Thermo Fisher Scientific, Hillsboro, OR, USA).

Comparisons

To evaluate the effects of systemic adrenaline and vPDT, we performed quantitative comparisons between different timepoints for CT and CVI. The remaining assessments and comparisons were qualitative in nature. Furthermore, for SD-OCT, FA, ICGA, and FAF images, observations at various time points were made against the baseline. Because histologic images were only available from a single time point after animal sacrifice and eye enucleation, all qualitative comparisons were between groups.

Investigative Ophthalmology & Visual Science

Downloaded from abstracts.iovs.org on 04/23/2024

Table 2. Changes in CT, LA, SA, and CVI After Systemic Adrenaline

	Choroidal Thickness µm (SD)		Luminal Area mm² (SD)		Stromal Area mm² (SD)		CVI (SD)	
	Subfoveal	Extrafoveal	Subfoveal	Extrafoveal	Subfoveal	Extrafoveal	Subfoveal	Extrafoveal
Baseline	207.60 (5.03)	194.00 (20.91)	32412 (2571)	44971 (8708)	21465 (2261)	26848 (9213)	0.602 (0.04)	0.607 (0.02)
% Change at week 4*	3.4%	2.2%	2.3%	−1.1%	4.3%	−3.1%	−4.2%	0.0%
P*	0.010	0.014	1.000	0.865	0.540	0.210	0.414	0.609
% Change at week 8†	3.9%	2.9%	16.0%	−1.7%	10.5%	1.1%	1.0%	0.5%
P†	0.007	0.009	0.030	0.886	0.080	0.650	0.820	0.800

* Week 4 data are compared against baseline data from 10 eyes of all five monkeys from Groups 2, 3, and 4.
† Week 8 data are compared against baseline data from six eyes of three (out of five) monkeys from Groups 2 and 4.

Statistical Evaluation

Statistical analyses were performed using R (Version 3.6.2). Continuous variables were summarized using means and standard deviations and categorical variables with counts and percentages. Comparisons across time points were performed using repeated measures analysis of variance.

Results

Effects of Systemic Adrenaline

We included observations of imaging studies from 10 eyes of five animals (groups 2, 3, and 4), sans group 1, which only received vPDT. In the animals which were assigned to vPDT and adrenaline (groups 3 and 4), only images obtained before the vPDT was performed were included in this section. The baseline and week 4 observations were obtained from all 10 eyes. The weeks 6 and 8 data were obtained from six eyes from groups 2 and 4. Observations of SD-OCT, FAF, FA, and ICGA at various time points were made against the baseline.

CT significantly increased at week 4 compared with the baseline in both the subfoveal (3.4%, $P = 0.010$) and extrafoveal regions (2.2%, $P = 0.014$). The increase was more marked after eight weeks of adrenaline therapy (subfoveal: 3.9%, $P = 0.007$; extrafoveal: 2.9%, $P = 0.009$) (Table 2). Within the choroid, the increase was seen predominantly in the subfoveal LA (16.0%, $P = 0.030$ at week 8 compared with baseline), whereas the increase in subfoveal SA was not statistically significant (10.5%, $P = 0.080$). There was no significant change in the CVI (Table 2).

The qualitative observations are as follows. On examination of the neurosensory retina, there was disruption and effacement of the ellipsoid zone (EZ) from week 6 onward and shallow subretinal fluid at week 8. Elongation and protrusion of photoreceptor outer segments, together with subretinal and intraretinal bright dots were also observed (Fig. 1).

None of the eyes developed leakage on FA. On ICGA, round hypocyanescent spots and surrounding leakage developed from week 4 onwards in three eyes (Fig. 2).

Histology. Only eyes that did not receive vPDT (Group 2) were used to evaluate the qualitative histologic effects of systemic adrenaline therapy and were compared against groups 1, 3, and 4. This captured a single time point after eight weeks of systemic adrenaline therapy after animal sacrifice and eye enucleation. The choroidal venules and choriocapillaris were dilated. There were also intracytoplasmic vacuoles and enlarged infoldings at the basal aspect of the RPE cells. The RPE cells were not noted to be significantly irregular in size and shape. No loss of tight junctions between RPE cells was observed (Fig. 3).

Effects of vPDT

SD-OCT, FAF, FA, and ICGA images that were obtained at two and four weeks after vPDT from 10 eyes of five monkeys (Groups 1, 3, and 4) were compared with the pre-vPDT images that were obtained immediately before vPDT. Therefore the pre-vPDT images that were used as baseline in groups 1, 3, and 4 were taken from baseline, post-adrenaline week 4, and post-adrenaline week 8, respectively.

Within the vPDT treatment zone (subfoveal region), there was a statistically significant reduction in CT in the subfoveal region at four weeks after vPDT compared with baseline (−7.5%, $P = 0.007$). Within the choroid, there was a more significant reduction in the SA (−18.0%, $P < 0.010$) compared with in the LA (−6.7%, $P = 0.150$) at week 4 after vPDT. As a result, there was a significant increase in the CVI after vPDT relative to the baseline at four weeks after vPDT (6.5%, $P < 0.010$). In the neurosensory retina, marked outer retinal changes were observed at two weeks after vPDT on SD-OCT. These included atrophy of outer retinal layers, severe EZ disruption, and irregular hyperreflective RPE thickening. These changes remained at four weeks after vPDT (See Table 3).

Outside the vPDT treatment zone (extrafoveal region), there was a borderline decrease in CT at week 4 compared with baseline (−6.0%, $P = 0.050$), which was accompanied by mild reduction in both LA and SA not reaching statistical significance. See Figure 4 for a comparison of SD-OCT changes between within and outside the vPDT treatment zone. Similar effects were observed after vPDT in eyes with (groups 3 and 4) and without (group 1) prior systemic adrenaline administration (See Table 3).

The qualitative observations are as follows. The treatment zone showed intense hypofluoresence on ICGA and FAF at two weeks after vPDT, which was surrounded by a ring of hyperfluorescence. This area appeared hyperfluorescent on FA. At four weeks after vPDT, the hypofluorescence on ICGA and FAF and the hyperfluorescence on FA partially resolved (Fig. 5).

Histology. Post-vPDT histologic changes in groups 1, 3, and 4 were evaluated in comparison to that in group 2, which received only systemic adrenaline. The qualitative histology findings included subretinal pigment-laden macrophages, pyknosis, and a monolayer of regenerated, flat, and hypopigmented RPE cells. In the outer retina, the outer nuclear layer was disrupted, and most of the photoreceptor cells were lost. The choroidal venules and choriocapillaris were narrow. In addition, the choroid had marked vascular endothelial growth factor staining. Likewise, similar histologic changes were observed after vPDT in eyes with (groups 3 and 4) and without (group 1) prior systemic adrenaline (Fig. 6).

Downloaded from abstracts.iovs.org on 04/23/2024

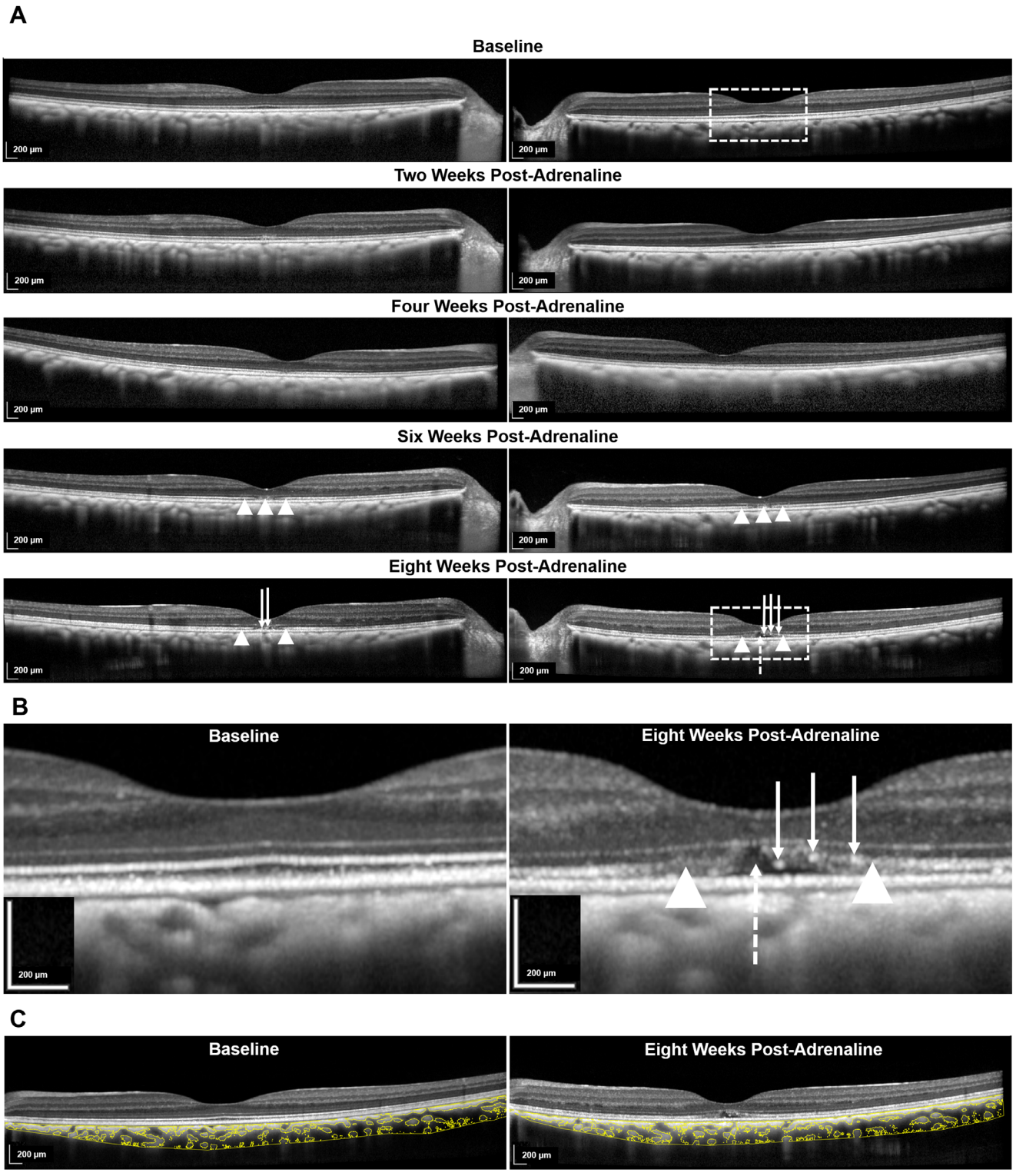

Figure 1. SD-OCT changes after systemic administration of adrenaline (group 4). (**A**) Longitudinal changes from baseline to eight weeks after administration of adrenaline in two eyes. From week 6 onward, disruption of the EZ was noted (indicated with *white arrowheads*). At eight weeks, in comparison with the baseline, there was elongation and protrusion of photoreceptor outer segments and intraretinal and subretinal bright dots (indicated with *solid white arrows*). There was also shallow subretinal fluid (indicated with *interrupted white arrow*). The areas of interest in the left eye at baseline and at week 8 are further demarcated with *interrupted white outlines* and are magnified in (**B**). (**B**) Magnified images comparing the left eye at week 8 after administration of adrenaline with baseline. (C) Binarization technique applied to the choroidal stromal and luminal components on the SD-OCT B-scan of the same eye at baseline and eight weeks after administration of adrenaline.

Investigative Ophthalmology & Visual Science

Downloaded from abstracts.iovs.org on 04/23/2024

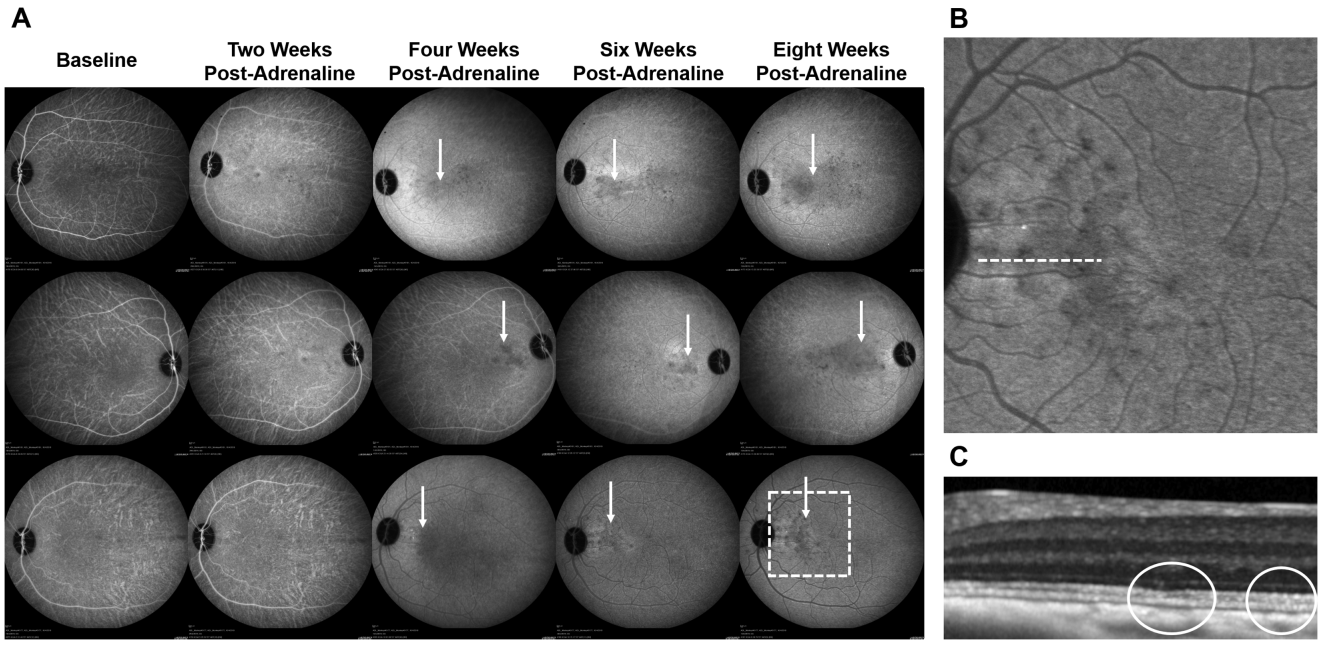

Figure 2. ICGA changes after systemic adrenaline (group 4). (**A**) On ICGA, round hypocyanescent spots and surrounding leakage developed from week 4 after administration of adrenaline onward in three eyes (indicated with *solid white arrows*). Area of interest in the last eye at week 8 is further demarcated with an interrupted white outline and is magnified in (**B**). (**B**) Magnified image of the area of interest in (**A**) demonstrating round hypocyanescent spots on ICGA. (**C**) Magnified SD-OCT B-scan of the region indicated with an *interrupted white line* in (**B**) demonstrating an effaced EZ (outlined in *solid white*).

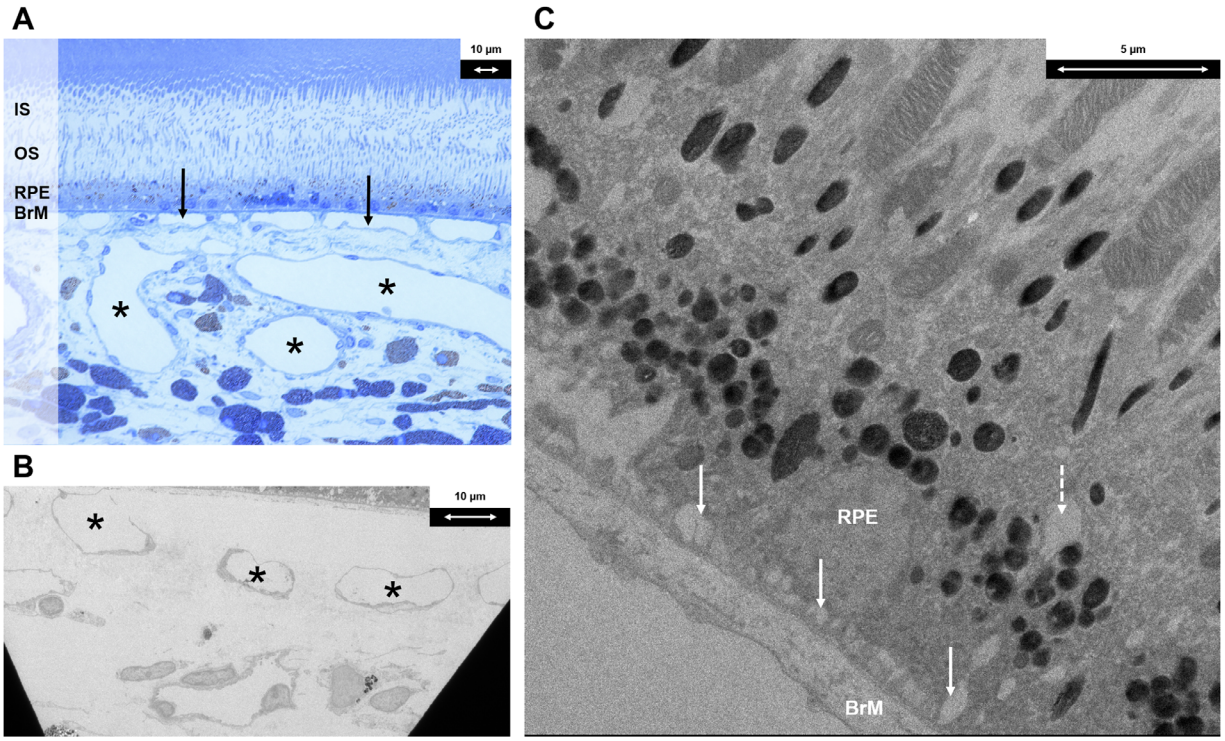

Figure 3. Histologic findings following systemic adrenaline (group 2). (**A**) Light microscopy section with toluidine blue stain at magnification × 40 demonstrating dilated choroidal venules (indicated with *black asterisks*) and choriocapillaris (indicated with *solid black arrows*). (**B**) Electron microscopy section at magnification × 440 demonstrating dilated choroidal venules (indicated with *black asterisks*). (**C**) Electron microscopy section at magnification × 1900 demonstrating an intracytoplasmic vacuole at the basal aspect of RPE cells (indicated with *interrupted white arrow*) and enlarged basal infoldings (indicated with *solid white arrows*). IS, inner segment; OS, outer segment; BrM, Bruch's membrane.

Investigative Ophthalmology & Visual Science

Downloaded from abstracts.iovs.org on 04/23/2024

Table 3. Changes in CT, LA, SA, and CVI After vPDT

	Choroidal Thickness µm (SD)		Luminal Area mm² (SD)		Stromal Area mm² (SD)		CVI (SD)	
	Subfoveal	Extrafoveal	Subfoveal	Extrafoveal	Subfoveal	Extrafoveal	Subfoveal	Extrafoveal
Baseline	190.70 (23.99)	175.50 (38.14)	32459.40 (4302.72)	44462.05 (8107.86)	23860 (2495)	33423 (3943)	0.589 (0.03)	0.610 (0.02)
% Change at week 2	−5.3%	−1.9%	−4.5%	−4.3%	−8.6%	−3.5%	5.8%	−0.3%
P	0.060	0.650	0.480	0.716	0.070	0.430	0.150	0.971
% Change at week 4*	−7.5%	−6.0%	−6.7%	−5.7%	−18.0%	−3.2%	6.5%	0.0%
P	0.007	0.050	0.150	0.560	<0.010	0.620	<0.010	0.636

* Week 4 data are compared against baseline data from 10 eyes of all five monkeys from groups 1, 3, and 4.

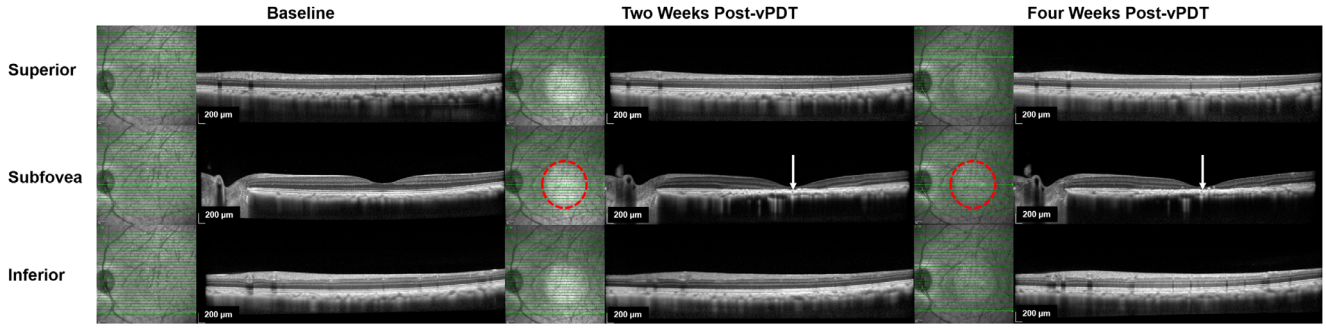

Figure 4. SD-OCT changes following vPDT (group 1). Comparison of SD-OCT changes within, superior to, and inferior to vPDT treatment zone at baseline, at two weeks, and at four weeks after vPDT. Near-infrared (NIR) images are shown adjacent to the corresponding SD-OCT B-scans to indicate the location of the B-scan in relation to the vPDT treatment zone. The boundary of the vPDT treatment zone is highlighted with an *interrupted red circle* in the NIR image, whereas the B scan location is indicated by the *solid horizontal green line*. At two and four weeks after vPDT, marked outer retinal changes were observed on SD-OCT (indicated with *solid white arrows*). These included atrophy of outer retinal layers, severe EZ disruption, and irregular hyperreflective RPE thickening. There were no significant changes observed on SD-OCT outside the vPDT treatment zone.

Discussion

In this study, we documented retinal and choroidal changes with multimodal imaging and histology after short-term systemic administration of adrenaline and subsequently vPDT. We elected to use a reduced dose of verteporfin 3 mg/m², which is half the recommended dose in humans with neovascular macular degeneration[32,33] and in the original experimental studies of verteporfin.[34,35] We also reduced the fluence of the infrared laser because this has been previously recognized as sufficient for the treatment of CSCR.[36]

In addition to traditional angiography, we incorporated SD-OCT with enhanced-depth imaging and novel quantitative metrics such as CVI to better understand the impact of adrenaline and vPDT on the luminal and stromal components of the choroid.

After the systemic administration of adrenaline, we observed several changes within the retina, RPE, and choroid, which recapitulate clinical findings in CSCR. These included the development of shallow neurosensory detachment, disruption of EZ, elongation and protrusion of photoreceptor outer segments, and subretinal and intraretinal bright dots. The earliest detectable change was an increase in subfoveal CT at week 4, which became more evident at week 8. Through using the image binarization technique, we found that changes in CT mainly arose because of an increase in the luminal component. The histologic finding of dilated choroidal vessels and choriocapillaris was consistent with the SD-OCT changes. These observations support previous reports that have proposed that a thickened choroid arises as a consequence of dilation in the large choroidal vessels (pachyvessels).[37–39]

In contrast to Yoshioka et al.,[24] we were unable to detect leakage on FA. On ICGA, we found hypocyanescent spots with surrounding leakage. Previous studies have reported similar dark spots in patients with CSCR and proposed that these may indicate regional choroidal filling delays and localized hypoperfusion.[40–43] Interestingly, Tittl et al.[43] demonstrated an abnormal subfoveal choroidal blood flow regulation and an inadequate vasoconstrictor response in chronic relapsing CSCR patients.

In the second part of this study, in eyes which were exposed to vPDT with and without the prior administration of systemic adrenaline, we observed reductions in CT both within and outside the treatment zone (albeit with a smaller change outside the treatment zone). This is concordant with the clinical findings after half-fluence vPDT in patients with CSCR.[2,3,44–46] Using image binarization, we demonstrated that the reduction in SA was greater than that of the LA. We propose that reduction in SA and volume may result from the resolution of exudate and inflammation.[47,48] In contrast to previous studies that have reported a reduction in CVI after vPDT,[27] we found a small increase in CVI of around 6.5%. The CVI is calculated as a proportion of the vascular component to the overall choroid volume. Therefore the reduction in the stromal volume without a corresponding change in the vessel volume could account for this small increase. Figure 7 illustrates the possible hypothesis for our observations. Alternatively, this may have arisen through differences in the study design because the timepoints selected for investigation after PDT may have resulted in the assessment reflecting different stages of choroidal remodeling. In this study, we chose to report the stromal changes at four weeks, whereas Izumi et al.[27] reported

Investigative Ophthalmology & Visual Science

Downloaded from abstracts.iovs.org on 04/23/2024

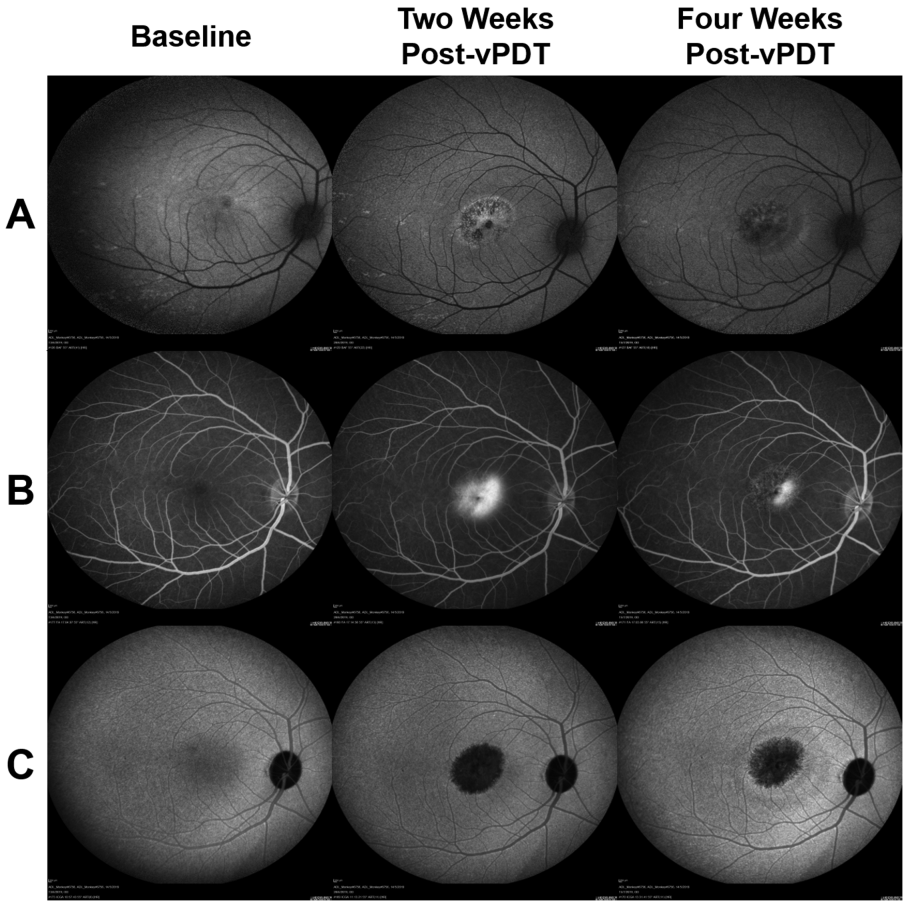

Figure 5. FA, ICGA, and FAF changes after vPDT (group 1). At two weeks after vPDT, the treatment zone showed intense hypofluoresence on (**A**) FAF and (**C**) ICGA, which was surrounded by a ring of hyperfluorescence; (**B**) This area appeared hyperfluorescent on FA. At four weeks after vPDT, the hypofluorescence on ICGA and FAF and the hyperfluorescence on FA are partially resolved.

predominant luminal changes at three months after half-dose PDT in eyes with CSCR.

We also observed marked outer retinal disruption affecting the outer nuclear layer, EZ, and RPE, especially from the SD-OCT and histologic findings. Intense hypoautofluorescence and hyperfluorescence on FA suggestive of RPE damage, which were most obvious at two weeks, showed partial recovery at four weeks after vPDT. These findings are also consistent with that reported in previous animal[49–52] and human studies.[53] The histology studies corroborated imaging findings that suggested damage to the outer retina and RPE (flat and hypopigmented RPE cells).[50]

In addition, the hypocyanescence on ICGA within the laser exposed treatment spot is suggestive of choriocapillaris nonperfusion, which showed partial recovery at four weeks along with histologic evidence of regeneration of choriocapillaris vascular endothelium. Although the adverse effects of vPDT including choroidal ischemia, secondary choroidal neovascularization, and RPE atrophy are known,[2,3] the severity of outer retinal and choriocapillaris damage despite the use of the reduced dose and fluence vPDT in our study was unexpected. Such dramatic alterations in retina and CT have not been observed in humans after vPDT even with a dose of 6 mg/m^2 verteporfin and a light fluence of 50 J/cm^2. It is generally believed that choriocapillaris hypoperfusion recovers within three months of vPDT, although some studies have reported hypoperfusion even at nine months.[47] Human studies with ICGA findings up to 24 months after vPDT suggested permanent closure of part of the choroidal vasculature.[54] Previous studies of vPDT in non-human primate models have mostly been performed after laser-induced choroidal neovascularization.[50,52] In contrast, the eyes in the current study had no or minimal subretinal fluid. This difference may explain the severe RPE and choriocapillaris damage in our study. Other studies that reported vPDT-induced outer retinal damage on primate models involved the use of higher doses of verteporfin administered repeatedly.[49–52] The retinal response to injury can involve migration, proliferation, necrosis, and pigmentary alteration of RPE cells.[55–58]

The key strength of this study is the concomitant evaluation of tomographic, angiographic, and histologic changes in the animal model of CSCR before and after vPDT. The cynomolgus monkey eye shares similarities in anatomy, function, and response to vPDT with the human eye. The limitations include the relatively small sample size, short follow-up period, and the absence of matched controls. The pre-vPDT baseline data represented data from monkeys that had received varying amounts of systemic adrenaline before undergoing vPDT. However, we noted that the post-vPDT effects were similar regardless of prior exposure to adrenaline. In addition, the intervals between vPDT and timepoints at which images were captured could have resulted in an inability to identify early changes in the

Downloaded from abstracts.iovs.org on 04/23/2024

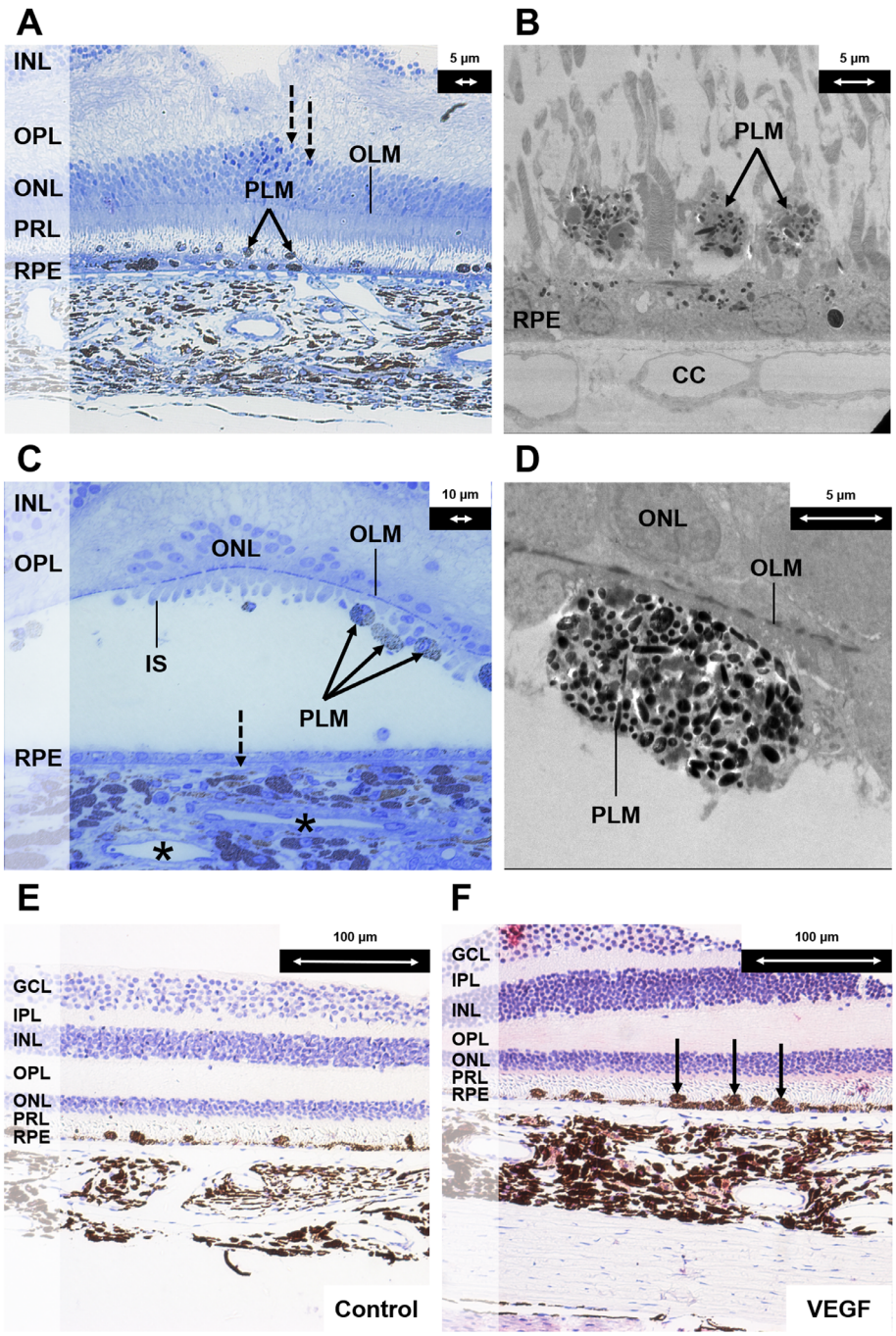

Figure 6. Histologic changes after half-dose half-fluence vPDT (groups 1, 3, and 4). (**A**) Light microscopy section with toluidine blue stain at magnification × 20 demonstrating the inner retina and choroid close to the laser spot. Pigment-laden macrophages were observed (indicated with *solid black arrows*). A monolayer of regenerated RPE cells with few melanin granules was seen. These cells were flatter in shape and hypopigmented because of the damage induced by vPDT (in contrast to the RPE cells in Figure 3A after administration of systemic adrenaline). A few pyknotic nuclei were seen in the ONL (indicated with *interrupted black arrows*). (**B**) Corresponding electron microscopy section at magnification × 890 demonstrating a monolayer of depigmented regenerating RPE cells after vPDT and pigment-laden macrophages (indicated with *solid black arrows*). (**C**) Composite image of light microscopy section with toluidine blue stain at magnification × 40 of the central part of the vPDT laser spot. The outer nuclear layer was disrupted. Most of the photoreceptor cells were lost. Few residual cone cells with the inner segments were seen at the foveal center. Pigment-laden macrophages were attached to the retina (indicated with *solid black arrows*). The RPE layer was composed by flat cells with few melanin granules. The lumens of the choriocapillaris were narrow (indicated with *interrupted black arrow*), and choroidal venules had narrow lumens (indicated with *black asterisks*). (**D**) Corresponding electron microscopy section at magnification × 1900 demonstrating a subretinal pigment-laden macrophage. (**E**) Light microscopy section at magnification × 20 as negative control for vascular endothelial growth factor (VEGF) staining of central area of vPDT. (**F**) Light microscopy section with VEGF antibody stain at magnification × 20 demonstrating marked VEGF staining in the choroidal stroma. There was positive staining of the subretinal macrophages (indicated with *solid black arrows*). There were also many round-shaped and spindle-shaped cells in the choroidal stroma compared with the control specimen. GCL, ganglion cell layer; IPL, inner plexiform layer; INL, inner nuclear layer; OPL, outer plexiform layer; ONL, outer nuclear layer; OLM, outer limiting membrane; PRL, photoreceptor layer; CC, choriocapillaris; PLM, pigment-laden macrophage.

Investigative Ophthalmology & Visual Science

Downloaded from abstracts.iovs.org on 04/23/2024

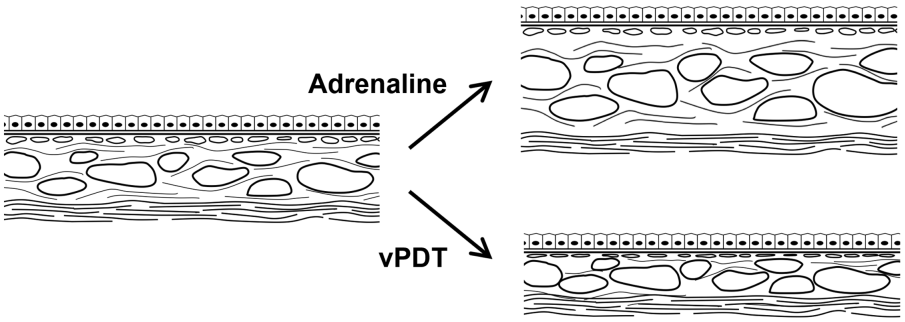

Figure 7. Schematic of histologic changes after vPDT. Systemic administration of adrenaline resulted in an increase in CT. This was predominantly the result of an increase in LA and, to a lesser extent, an increase in SA. After vPDT, marked decrease in CT within the vPDT treatment spot resulted mainly from a reduction in SA and a less marked reduction in LA.

outer retina, RPE, and choroid because these may have been missed with recovery. We also have no longer-term data. We also did not examine functional effects using electroretinography to assess their relationship with anatomic changes.

Notably, the absence of FA leakage in this study calls into question whether a true CSCR model was created in this study. Although there was no FA leakage, the observed features as described are suggestive of outer retinal changes, RPE dysfunction, and choroidal congestion. This would constitute a pachychoroid model at the very least. CSCR resides in the pachychoroid disease spectrum. Multimodal imaging in other studies have demonstrated that RPE disease occurs at locations that coincide with regional choroidal hyperpermeability and focal choroidal thickening.[59–61] We further postulate that had the monkeys been kept for a longer time, the observed choroidal changes would have progressed to FA leakage.

In summary, this study has provided valuable information regarding the tomographic, angiographic, and histologic changes in the choroid and retina of cynomolgus monkey eyes after induction of experimental CSCR by systemic administration of adrenaline and subsequent treatment with vPDT. The characterization of changes in the outer retina, RPE, and the choroidal angioarchitecture show that this model is relevant to the study of CSCR, therapeutic effects of vPDT, and potential therapeutic interventions affecting the choroid.

Acknowledgments

Supported by Duke/Duke-NUS Research Collaborations Grant: Duke/Duke-NUS/RECA(Pilot)2016/0020, Biomedical Research Council Singapore Grant: SPF2014/002, National Medical Research Council Open Fund Large Collaborative Grant: NMRC/LCG/004/2018, NMRC/CG-INCEPTOR/Pre-Clinical Core Platform/2017_SERI.

Disclosure: **K.X. Cheong,** None; **V.A. Barathi,** None; **K.Y.C. Teo,** None; **U. Chakravarthy,** None; **S.B.B. Tun,** None; **J.M. Busoy,** None; **C.E.H. Ho,** None; **R. Agrawal,** None; **K. Takahashi,** None; **C.M.G. Cheung,** None

References

1. Cheung CMG, Lee WK, Koizumi H, Dansingani K, Lai TYY, Freund KB. Pachychoroid disease. *Eye (Lond)*. 2019;33:14–33.
2. Romano MR, Parolini B, Allegrini D, Mickalewska Z, Adelman R, Bonovas S, Bopp S, EVRS study group. An international collaborative evaluation of central serous chorioretinopathy: different therapeutic approaches and review of literature. The European Vitreoretinal Society central serous chorioretinopathy study [published online ahead of print December 6, 2019]. *Acta Ophthalmol*, https://doi.org/10.1111/aos.14319.
3. Nicholson B, Noble J, Forooghian F, Meyerle C. Central serous chorioretinopathy: update on pathophysiology and treatment. *Surv Ophthalmol*. 2013;58:103–126.
4. Kitzmann AS, Pulido JS, Diehl NN, Hodge DO, Burke JP. The incidence of central serous chorioretinopathy in Olmsted County, Minnesota, 1980-2002. *Ophthalmology*. 2008;115:169–173.
5. Spaide RF, Campeas L, Haas A, et al. Central serous chorioretinopathy in younger and older adults. *Ophthalmology*. 1996;103:2070–2080.
6. Harada T, Harada K. Six cases of central serous choroidopathy induced by systemic corticosteroid therapy. *Doc Ophthalmol*. 1985;60:37–44.
7. Wakakura M, Ishikawa S. Central serous chorioretinopathy complicating systemic corticosteroid treatment. *Br J Ophthalmol*. 1984;68:329–331.
8. Garg SP, Dada T, Talwar D, Biswas NR. Endogenous cortisol profile in patients with central serous chorioretinopathy. *Br J Ophthalmol*. 1997;81(11):962–964.
9. Ahnoux-Zabsonre A, Quaranta M, Mauget-Faysse M. [Prevalence of Helicobacter pylori in central serous chorioretinopathy and diffuse retinal epitheliopathy: a complementary study]. *J Fr Ophtalmol*. 2004;27:1129–1133.
10. Weenink AC, Borsje RA, Oosterhuis JA. Familial chronic central serous chorioretinopathy. *Ophthalmologica*. 2001;215:183–187.
11. Wynn PA. Idiopathic central serous chorioretinopathy—a physical complication of stress? *Occup Med (Lond)*. 2001;51:139–140.
12. Yannuzzi LA. Type A behavior and central serous chorioretinopathy. *Trans Am Ophthalmol Soc*. 1986;84:799–845.
13. Uyama M, Matsunaga H, Matsubara T, Fukushima I, Takahashi K, Nishimura T. Indocyanine green angiography and pathophysiology of multifocal posterior pigment epitheliopathy. *Retina*. 1999;19:12–21.
14. Yannuzzi LA. Central serous chorioretinopathy: a personal perspective. *Am J Ophthalmol*. 2010;149:361–363.
15. Chan WM, Lam DS, Lai TY, Tam BS, Liu DT, Chan CK. Choroidal vascular remodelling in central serous chorioretinopathy after indocyanine green guided photodynamic therapy with verteporfin: a novel treatment at the primary disease level. *Br J Ophthalmol*. 2003;87:1453–1458.

Downloaded from abstracts.iovs.org on 04/23/2024

16. Yannuzzi LA, Slakter JS, Gross NE, et al. Indocyanine green angiography-guided photodynamic therapy for treatment of chronic central serous chorioretinopathy: a pilot study. *Retina*. 2003;23:288–298.
17. Bae SH, Heo JW, Kim C, et al. A randomized pilot study of low-fluence photodynamic therapy versus intravitreal ranibizumab for chronic central serous chorioretinopathy. *Am J Ophthalmol*. 2011;152:784–792.e2.
18. Ting DSW, Yanagi Y, Agrawal R, et al. Choroidal remodeling in age-related macular degeneration and polypoidal choroidal vasculopathy: A 12-month prospective study. *Sci Rep*. 2017;7:7868.
19. Yanagi Y, Ting DSW, Ng WY, et al. Choroidal vascular hyperpermeability as a predictor of treatment response for polypoidal choroidal vasculopathy. *Retina*. 2018;38:1509–1517.
20. Teo KYC, Yanagi Y, Lee SY, et al. Comparison of optical coherence tomography angiographic changes after antivascular endothelial growth factor therapy alone or in combination with photodynamic therapy in polypoidal choroidal vasculopathy. *Retina*. 2018;38:1675–1687.
21. Yoshioka H, Katsume Y, Akune H. Experimental central serous chorioretinopathy in monkey eyes: fluorescein angiographic findings. *Ophthalmologica*. 1982;185:168–178.
22. Yoshioka H, Katsume Y, Ishibashi R. Experimental central serous chorioretinopathy. II: Further clinical findings. *Kurume Med J*. 1981;28:189–196.
23. Yoshioka H, Katsume Y. Experimental central serous chorioretinopathy. III: Ultrastructural findings. *Jpn J Ophthalmol*. 1982;26:397–409.
24. Yoshioka H, Katsume Y, Akune H, Nagasaki H. Experimental central serous chorioretinopathy. IV: Fluorescein angiography and electron microscopy during spontaneous healing process. *Kurume Med J*. 1984;31:89–99.
25. Agrawal R, Gupta P, Tan KA, Cheung CM, Wong TY, Cheng CY. Choroidal vascularity index as a measure of vascular status of the choroid: Measurements in healthy eyes from a population-based study. *Sci Rep*. 2016;6:21090.
26. Wei X, Ting DSW, Ng WY, Khandelwal N, Agrawal R, Cheung CMG. Choroidal vascularity index: a novel optical coherence tomography based parameter in patients with exudative age-related macular degeneration. *Retina*. 2017;37:1120–1125.
27. Izumi T, Koizumi H, Maruko I, et al. Structural analyses of choroid after half-dose verteporfin photodynamic therapy for central serous chorioretinopathy. *Br J Ophthalmol*. 2017;101:433–437.
28. Sonoda S, Sakamoto T, Kuroiwa N, et al. Structural changes of inner and outer choroid in central serous chorioretinopathy determined by optical coherence tomography. *PLoS One*. 2016;11:e0157190.
29. Schneider CA, Rasband WS, Eliceiri KW. NIH Image to ImageJ: 25 years of image analysis. *Nat Methods*. 2012;9:671–675.
30. Schindelin J, Arganda-Carreras I, Frise E, et al. Fiji: an open-source platform for biological-image analysis. *Nat Methods*. 2012;9:676–682.
31. Nivison-Smith L, Khandelwal N, Tong J, Mahajan S, Kalloniatis M, Agrawal R. Normal aging changes in the choroidal angioarchitecture of the macula. *Sci Rep*. 2020;10:10810.
32. Treatment of age-related macular degeneration with photodynamic therapy (TAP) Study Group. Photodynamic therapy of subfoveal choroidal neovascularization in age-related macular degeneration with verteporfin: one-year results of 2 randomized clinical trials—TAP report. *Arch Ophthalmol*. 1999;117:1329–1345.
33. Schmidt-Erfurth U, Miller JW, Sickenberg M, et al. Photodynamic therapy with verteporfin for choroidal neovascularization caused by age-related macular degeneration: results of retreatments in a phase 1 and 2 study. *Arch Ophthalmol*. 1999;117:1177–1187.
34. Yannuzzi LA, Slakter JS, Gross NE, et al. Indocyanine green angiography-guided photodynamic therapy for treatment of chronic central serous chorioretinopathy: a pilot study. *Retina*. 2003;23:288–298.
35. Taban M, Boyer DS, Thomas EL. Chronic central serous chorioretinopathy: photodynamic therapy. *Am J Ophthalmol*. 2004;137:1073–1080.
36. Karim SP, Adelman RA. Profile of verteporfin and its potential for the treatment of central serous chorioretinopathy. *Clin Ophthalmol*. 2013;7:1867–1875.
37. Yang L, Jonas JB, Wei W. Choroidal vessel diameter in central serous chorioretinopathy. *Acta Ophthalmol*. 2013;91:e358–e362.
38. Chung YR, Kim JW, Kim SW, Lee K. Choroidal thickness in patients with central serous chorioretinopathy: assessment of Haller and Sattler layers. *Retina*. 2016;36:1652–1657.
39. Agrawal R, Chhablani J, Tan KA, Shah S, Sarvaiya C, Banker A. Choroidal vascularity index in central serous chorioretinopathy. *Retina*. 2016;36:1646–1651.
40. Kitaya N, Nagaoka T, Hikichi T, et al. Features of abnormal choroidal circulation in central serous chorioretinopathy. *Br J Ophthalmol*. 2003;87:709–712.
41. Saito M, Saito W, Hashimoto Y, et al. Macular choroidal blood flow velocity decreases with regression of acute central serous chorioretinopathy. *Br J Ophthalmol*. 2013;97:775–780.
42. Tittl M, Polska E, Kircher K, et al. Topical fundus pulsation measurement in patients with active central serous chorioretinopathy. *Arch Ophthalmol*. 2003;121:975–978.
43. Tittl M, Maar N, Polska E, Weigert G, Stur M, Schmetterer L. Choroidal hemodynamic changes during isometric exercise in patients with inactive central serous chorioretinopathy. *Invest Ophthalmol Vis Sci*. 2005;46:4717–4721.
44. Maruko I, Iida T, Sugano Y, Ojima A, Ogasawara M, Spaide RF. Subfoveal choroidal thickness after treatment of central serous chorioretinopathy. *Ophthalmology*. 2010;117:1792–1799.
45. Maruko I, Iida T, Sugano Y, Furuta M, Sekiryu T. One-year choroidal thickness results after photodynamic therapy for central serous chorioretinopathy. *Retina*. 2011;31:1921–1927.
46. Shin JY, Woo SJ, Yu HG, Park KH. Comparison of efficacy and safety between half-fluence and full-fluence photodynamic therapy for chronic central serous chorioretinopathy. *Retina*. 2011;31:119–126.
47. Kinoshita T, Mitamura Y, Mori T, et al. Changes in choroidal structures in eyes with chronic central serous chorioretinopathy after half-dose photodynamic therapy. *PLoS One*. 2016;11:e0163104.
48. Park W, Kim M, Kim RY, Park YH. Comparing effects of photodynamic therapy in central serous chorioretinopathy: full-dose versus half-dose versus half-dose-half-fluence. *Graefes Arch Clin Exp Ophthalmol*. 2019;257:2155–2161.
49. Tzekov R, Lin T, Zhang KM, et al. Ocular changes after photodynamic therapy. *Invest Ophthalmol Vis Sci*. 2006;47:377–385.
50. Husain D, Kramer M, Kenny AG, et al. Effects of photodynamic therapy using verteporfin on experimental choroidal neovascularization and normal retina and choroid up to 7 weeks after treatment. *Invest Ophthalmol Vis Sci*. 1999;40:2322–2331.
51. Reinke MH, Canakis C, Husain D, et al. Verteporfin photodynamic therapy retreatment of normal retina and choroid in the cynomolgus monkey. *Ophthalmology*. 1999;106:1915–1923.

Investigative Ophthalmology & Visual Science

Downloaded from abstracts.iovs.org on 04/23/2024

52. Kramer M, Miller JW, Michaud N, et al. Liposomal benzoporphyrin derivative verteporfin photodynamic therapy: selective treatment of choroidal neovascularization in monkeys. *Ophthalmology*. 1996;103:427–438.
53. Schlötzer-Schrehardt U, Viestenz A, Naumann GO, Laqua H, Michels S, Schmidt-Erfurth U. Dose-related structural effects of photodynamic therapy on choroidal and retinal structures of human eyes. *Graefes Arch Clin Exp Ophthalmol*. 2002;240(9):748–757.
54. Schmidt-Erfurth UM, Michels S. Changes in confocal indocyanine green angiography through two years after photodynamic therapy with verteporfin. *Ophthalmology*. 2003;110:1306–1314.
55. Marshall J. Interactions between sensory cells, glial cells and the retinal pigment epithelium and their response to photocoagulation. *Dev Ophthalmol*. 1981;2:308–317.
56. Smiddy WE, Fine SL, Quigley HA, et al. Cell proliferation after laser photocoagulation in primate retina. An autoradiographic study. *Arch Ophthalmol*. 1986;104:1065–1069.
57. Wallow IHL, Tso MOM. Repair after xenon arc photocoagulation. 3. An electron microscopic study of the evolution of retinal lesions in rhesus monkeys. *Am J Ophthalmol*. 1973;75:957–972.
58. Valentino TL, Kaplan HJ, Del Priore LV, et al. Retinal pigment epithelial repopulation in monkeys after submacular surgery. *Arch Ophthalmol*. 1995;113:932–938.
59. Cheung CMG, Lee WK, Koizumi H, et al. Pachychoroid disease. *Eye (Lond)*. 2019;33:14–33.
60. Guyer DR, Yannuzzi LA, Slakter JS, et al. Digital indocyanine green videoangiography of central serous chorioretinopathy. *Arch Ophthalmol*. 1994;112:1057–1062.
61. Spaide RF, Klancnik JM, Jr. Fundus autofluorescence and central serous chorioretinopathy. *Ophthalmology*. 2005;112:825–833.

Investigative Ophthalmology & Visual Science

Downloaded from abstracts.iovs.org on 04/23/2024